Michigan State University

National Superconducting Cyclotron Laboratory

TIME SCALE FOR EMISSION OF INTERMEDIATE MASS FRAGMENTS IN $^{36}Ar + ^{197}Au$ COLLISIONS AT E/A = 35 MeV

Y.D. KIM, R.T. de SOUZA, D.R. BOWMAN, N. CARLIN, C.K. GELBKE, W.G. GONG, W.G. LYNCH, L. PHAIR, M.B. TSANG, F. ZHU, and S. PRATT

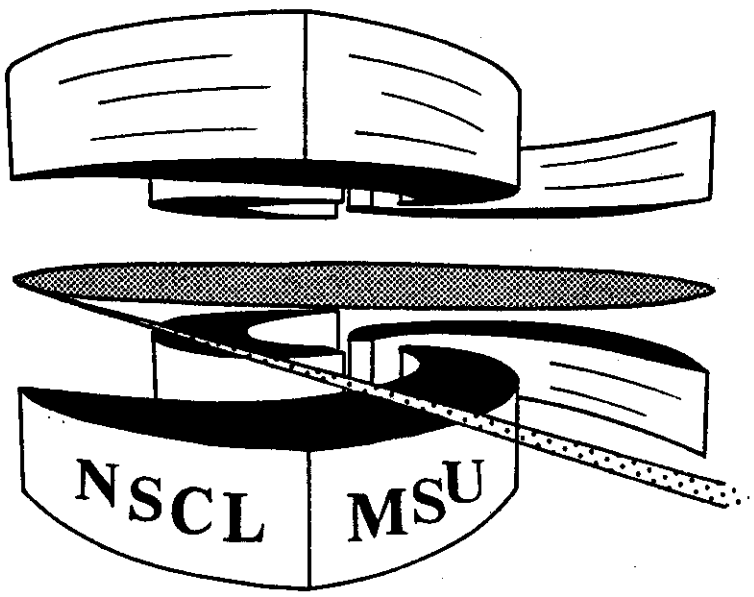

MSUCL-780 **MAY 1991**

MSUCL-780
May, 1991

"Tim Scale for Emission of Intermediate Mass Fragments In $^{36}Ar+^{197}Au$ Collisions at E/A=35 MeV"

Y. D. Kim, R. T. de Souza, D. R. Bowman, N. Carlin,† C. K. Gelbke, W. 4. Gong, W. 4. Lynch, L. Phalr, M. B. Tsang, and F. Zhu

National Superconductlng Cyclotron Laboratory

and Department of Physics and Astronomy

Michigan State University, East Lansing, MI. 46624, USA

S. Pratt

Department of Physics, University of Wisconsin, Madison, WI 53706, USA

Abstract

Two-fragment (Be-Be, 8-8, and C-C) correlation functions were measured at small relative momenta for noncompound fragment emission in $^{36}Ar+^{197}Au$ collisions at E/A=35 MeV. Interpretation of the experimental correlation functions In terms of flnal-state Coulomb-interaction models indicate average fragment emission times of about 100-200 fm/c.

PACS index: 25.70.Gh, 25.70.Lm, 25.70.Np

---

† Present address: Instltuto de Física, Universidade de São Paulo, C. Postal 20516, CEP 01498, Silo Paulo, Brazil

Final states produced in central nucleus-nucleus collisions evolve dramatically with incident energy from single or binary fragment exit channels to a complete disintegration of the nuclear system into light particles and intermediate mass fragments [1-3]. The study of multifragment final states over a broad range of incident energy may provide information about nuclear phase transitions and the equation of state of nuclear matter at low densities [4,5], provided that multifragment disintegrations are related to bulk instabilities of nuclear matter at low density [3-11]. Such disintegrations should occur on short time scales, $\tau \lesssim 100$ fm/c, characteristic of the growth of density fluctuations in the nuclear medium. Alternatively, multifragment final states can also be produced via sequences of binary disintegrations predicted by generalized models of compound nucleus decay [12-14] governed by different time scales. For example, time intervals between emission of two carbon fragments from equilibrated heavy nuclei (A=226, Z=93) of 700 MeV excitation energy are calculated [14] to be of the order of $\tau \approx 300$ fm/c. Experimental information about the time scale of fragment emission may help distinguish between such different fragment production mechanisms [15-18]. In this letter, we apply the technique of intensity interferometry [15,19-22] to multifragment decays and extract time scales for the emission of Z=4-6 fragments in the $^{36}Ar+^{197}Au$ reaction at E/A=35 MeV.

The experiment was performed with an ^{36}Ar beam of energy, E/A=35 MeV, and intensity, $I \approx 10^8$ particles per second, produced by the K500 cyclotron of the NSCL at Michigan State University. The areal density of the gold target was 1 mg/cm^2. Light particles and complex fragments were detected with the MSU Miniball [23] with an angular coverage of θ_{lab}=16°-160° and solid angle of 85%

of 4π. Particles punching through the 4 mg/cm^2 plastic scintillator foils were identified by charge up to Z=18 and by mass for H and He isotopes [23,24]. The approximate energy thresholds are $E_{th}/A \approx 2$ MeV for Z=3, $E_{th}/A \approx 3$ MeV for Z=10, and $E_{th}/A \approx 4$ MeV for Z=18 fragments. Energy calibrations, accurate to within 5% were obtained by measuring the elastic scattering of ^{10}B, ^{12}C and ^{16}O beams from an ^{197}Au target at incident energies of $E(^{10}B)/A$=15 MeV; $E(^{12}C)/A$ = 6, 8, 13, and 20 MeV; and $E(^{16}O)/A$ = 6, 8, 16, and 20 MeV. Random coincidences were negligible at the above intensity.

Two-fragment correlation functions were constructed from intermediate mass fragments detected in rings 2 and 3. Detectors in these rings are centered at polar angles of θ_2=19.5° and θ_3=27° and subtend intervals in polar and azimuthal angles of $\Delta\theta_2$=7°, $\Delta\phi_2$=22.5° and $\Delta\theta_3$=8°, $\Delta\phi_3$=18°, respectively. The inclusive energy spectra of Be, B, and C fragments detected in these rings are shown in Fig. 1. The shapes of the energy spectra are similar to those observed in other heavy-ion induced reactions at comparable energies and are indicative of large contributions from noncompound emission mechanisms, see e.g. ref. [25]. The detection of one or two intermediate mass fragments in rings 2 or 3 selected events with a most probable charged particle multiplicity of about 10 which is close to the location of the central collision peak of the inclusive multiplicity distribution.

We define the experimental two-fragment correlation function, R(q), in terms of the coincidence yield, $Y_{12}(\vec{p}_1,\vec{p}_2)$, and the single particle yields, $Y_1(\vec{p}_1)$ and $Y_2(\vec{p}_2)$ [20]:

$$\Sigma Y_{12}(\vec{p}_1,\vec{p}_2) = C[1+R(q)]\Sigma Y_1(\vec{p}_1)Y_2(\vec{p}_2) \ . \qquad (1)$$

Here, $\vec{p}_1$ and $\vec{p}_2$ are the laboratory momenta of fragments 1 and 2; $q=\frac{1}{2}|\vec{p}_1-\vec{p}_2|$ is the relative momentum of the particle pair, and C is a normalization constant determined by the requirement that $\langle R(q)\rangle=0$ at large relative momenta where the final state interaction between the emitted fragments can be neglected. In this analysis, we approximated the fragment mass number as twice the atomic number unless stated otherwise.

Experimental two-fragment correlation functions are shown in Fig. 2. The top, center, and bottom panels show Be-Be, B-B, and C-C correlation functions [24]. The left panels present inclusive correlation functions and the right panels show correlation functions gated by the requirement $N\geq 9$ and $P/A>150$ MeV/c, where N denotes the total number of charged particles detected in the Miniball and P/A is the total momentum per nucleon of the coincident fragment pair. All correlation functions exhibit pronounced minima at $q\approx 0$ MeV/c which can be attributed to the repulsive final state Coulomb interaction between the emitted fragments. The correlation functions gated by $N\geq 9$ and $P/A>150$ MeV/c are similar in shape to the inclusive correlation functions, indicating that this gate does not select significantly different emission times.

The curves shown in the figure represent calculations with the formalism of ref. [22], generalized to the case of two intermediate mass fragments. Since average fragment separations are expected to be larger than the range of the nuclear force, we neglect nuclear interactions and treat the final-state

Coulomb interaction between the two coincident fragments classically. In this approximation, the two-fragment correlation function can be expressed as [26]

$$1+R(q) = \frac{\int d^3r\, F_{\vec{p}}(\vec{r})[1 - \frac{2\mu Z^2 e^2}{q^2 r}]^{\frac{1}{2}}}{\int d^3r\, F_{\vec{p}}(\vec{r})}, \qquad (2)$$

where, Z is the fragment charge, $\mu=\frac{1}{2}m$ is the reduced mass, and $F_{\vec{p}}(\vec{r})$ is the distribution of relative coordinates between particles, each emitted with momentum $\vec{p}=\frac{1}{2}\vec{P}$ (see Eqs. 23 and 24 of ref. [22]). For the calculations presented in Fig. 2, $F_{\vec{p}}(\vec{r})$ was calculated by assuming the fragments to be emitted from incomplete fusion residues moving with a source velocity $V_S=0.035c$, a value consistent with the systematics of linear momentum transfer for reactions producing heavy reaction residues [27,28]. For simplicity, the emitted fragments and the heavy reaction residues were assumed to be separated by $R_S=12$ fm at the time of emission. The distribution of emission points on the surface of the heavy reaction residue was taken from Lambert's Law for surface emission. An exponential probability distribution of emission times was assumed, $P(t) = (\frac{1}{\tau})e^{-t/\tau}$, with mean emission times τ given in the figure [29]. The simulated energy and angular distributions of the fragments were chosen in accordance with the measured single fragment distributions.

The comparison between measured and calculated correlation functions in Fig. 2 indicates that the inclusive correlation functions are reasonably consistent with mean emission times of about $\tau\approx$100-200 fm/c. The correlation functions gated by N$\geq$9 and P/A>150 MeV/c appear to indicate slightly shorter emission time scales.

In our calculations, we neglect the possibility that highly excited primary fragments could undergo sequential decays by particle emission. Such decays may be expected to attenuate the minimum at q≈0 MeV/c [30]. It is, therefore, possible that our analysis yields mean emission times which are slightly larger than those of the primary fragments. Our data seem to indicate slightly larger emission times for Be fragments than for B or C fragments. Furthermore, the calculations reproduce the Be-Be correlation function less well than the B-B or C-C correlation functions. It is interesting to speculate that these observations could be related to enhanced feeding of Be nuclei. Additional experimental information concerning the magnitude of sequential feeding would help resolve this issue.

Figure 3 illustrates systematic uncertainties introduced by our apparatus and data analysis. The curves in panels (a) and (b) show the theoretical B-B correlation functions already presented in the left center panel of Fig. 2. The solid and open points in panel (a) show the correlation functions for τ=100 and 500 fm/c, respectively, filtered by the response of our apparatus. The resulting distortions are of minor importance. (The instrumental distortions at very small values of q are mainly due to the finite angular resolution of the apparatus; uncertainties in energy calibration are small in comparison.) Panel (b) illustrates errors which could arise from the unknown mass of the detected fragments. The solid and open points show experimental B-B correlation functions constructed by assuming A=10 and A=11, respectively, for the mass of the detected boron fragments. The sensitivity of the calculation to uncertainties of the velocity and size of the emitting source is

illustrated in panels (c) and (d). None of these uncertainties changes the extracted lifetimes by more than 50%.

The derivation of Eq. 2 is based upon the assumption that dynamical correlations and distortions in the Coulomb field of the residual nucleus can be neglected. For the present reaction, the charged particle multiplicities are sufficiently low to virtually guarantee the survival of a heavy reaction residue (which might subsequently fission). To assess the influence of the Coulomb field of the heavy reaction residue, we have performed three-body Coulomb trajectory calculations which consider the sequential emission of two carbon nuclei from the surface of a residual nucleus initially with charge number Z_S=93, mass number A_S=226, and velocity V_S=0.035c. As before, we assumed an exponential probability distribution of emission times and fragment energy distributions consistent with the measured carbon spectrum. For the emission of the second fragment, we required a minimum initial separation of 7.4 fm from the first fragment. The response of the experimental apparatus was included. In Fig. 4a, the results of these calculations (curves) are compared to the inclusive C-C correlation function (points). The three-body Coulomb trajectory calculations predict wider minima in the correlation functions than the calculations based upon Eq. 2, and the agreement with the data is slightly worse. Nevertheless, the calculations are in fair agreement with the experimental correlation functions for emission times of the order of 100-200 fm/c. In Fig. 4b, we compare calculations for τ=200 fm/c. The curve shows the calculation with Eq. 2 and the solid points show the results of the three-body trajectory calculation. The discrepancy between the two model calculations is largely caused by dynamical correlations caused by the recoil of the heavy

reaction residue which is included in the trajectory calculation, but not in Eq. 2. Indeed, the calculation with Eq. 2 is in rather good agreement with three-body calculations when the recoil of the heavy target residue is artificially reduced by increasing its mass to A_S=5000 while keeping its charge and radius constant (open points). These calculations suggest that the detailed shape of the predicted correlation function is influenced by the reaction dynamics and that additional insight may be gained by calculating correlation functions from more realistic reaction models.

In summary, two-fragment correlation functions for the $^{36}Ar+^{197}Au$ reaction indicate mean fragment emission times of the order of 100-200 fm/c. These mean emission times are shorter than those extracted previously [15,18,29] for reactions induced by lighter projectiles. For the present reaction, the emission times are slightly shorter than those calculated from evaporation models [14].

The authors gratefully acknowledge the calculation of IMF emission times from compound nuclei by Prof. W.A. Friedman. This work is based upon work supported by the National Science Foundation under Grant numbers PHY-86-11210, PHY-89-13815. WGL acknowledges the receipt a of U.S. Presidential Young Investigator Award and NC acknowledges partial support by the FAPESP, Brazil.

References

1. K.G.R. Doss et al., Phys. Rev. Lett. 59, 2720 (1987).
2. W. Lynch, Ann. Rev. Nucl. Part. Sci., 37, 493 (1987).
3. D.H.E. Gross, Rep. Prog. Phys. 53, 605 (1990).
4. L.P. Cernai and J. Kapusta, Phys. Reports 131, 223 (1986).
5. E. Suraud, Nucl. Phys. A495, 73 (1989).
6. G. Bertsch and P.J. Siemens, Phys. Lett. 126B, 9 (1983).
7. T.J. Schlagel, and V.R. Pandharipande, Phys. Rev. C36, 162 (1987).
8. W. Bauer et al., Phys. Rev. Lett. 58, 863 (1987).
9. K. Sneppen et al., Nucl. Phys. A480, 342 (1988).
10. J. Aichelin et al., Nucl. Phys. A488, 437c (1988).
11. D.H. Boal and J.N. Glosli, Phys. Rev. C37, 91 (1988); Phys. Rev. C42, R502 (1990).
12. L.G. Moretto, Nucl. Phys. A247, 211 (1975).
13. W.A. Friedman and W.G. Lynch, Phys. Rev. C28, 16 (1983); C28, 950 (1983).
14. W.A. Friedman, Phys. Rev. Lett. 60, 2125 (1988); Phys. Rev. C40, 2055 (1989); Phys. Rev. C42, 667 (1990); and private communication.
15. R. Trockel et al., Phys. Rev. Lett. 59, 2844 (1987).
16. J.A. Lopez and J. Randrup, Nucl. Phys. A491, 477 (1989).
17. D. Cebra et al., Phys. Rev. Lett. 64, 2246 (1990).
18. R. Bougault et al., Phys. Lett. B232, 291 (1989).
19. S.E. Koonin, Phys. Lett. 70B, 43 (1977).
20. D.H. Boal et al., Rev. Mod. Phys. 62, 553 (1990).
21. P.A. DeYoung et al., Phys. Rev. C41, R1885 (1990).
22. W.G. Gong et al., Phys. Rev. C43, 781 (1991).

23. R.T. de Souza et al., Nucl. Instr. and Meth. A295, 109 (1990).

24. Double hits by α-particles resulting, for example, from ^{8}Be decays were identified by pulse shape discrimination and excluded from the data presented in Figs. 1-4.

25. D.E. Fields et al., Phys. Lett. B220, 356 (1989).

26. We have verified that Eq. 2 provides an excellent approximation by also performing more time-consuming calcalutions utilizing a partial wave expansion for the relative Coulomb wave function.

27. M. Fatyga et al., Phys. Rev. Lett. 55, 1376 (1985).

28. Y. Cassagnou et al., Proceedings of the Symposium on Nuclear Dynamics and Nuclear Disassembly, held at Dallas, Texas, April 1989, edited by J. Natowitz, World Scientific, Singapore 1989, p. 386.

29. The mean emission time, τ, and the "half-life" for IMF emission, $\tau_{IMF-IMF}$, defined in ref. [15], are related as: $\tau=1.44\tau_{IMF-IMF}$.

30. H.W. Barz et al., Phys. Lett. B244, 161 (1990).

Figure Captions:

Fig. 1: Inclusive energy spectra of Be, B, and C fragments for the $^{36}Ar+^{197}Au$ reaction at E/A=35 MeV.

Fig. 2: Inclusive (left hand panels) and gated (right hand panels) two-fragment correlation functions at small relative momenta. The calculations are explained in the text.

Fig. 3: Estimates of experimental and theoretical uncertainties; a detailed discussion is given in the text.

Fig. 4: Panel (a): Comparison of inclusive C-C correlation functions to three-body Coulomb trajectory calculations. Panel (b): Correlation functions calculated from Eq. 2 (curve) and from three-body trajectory calculations (points).

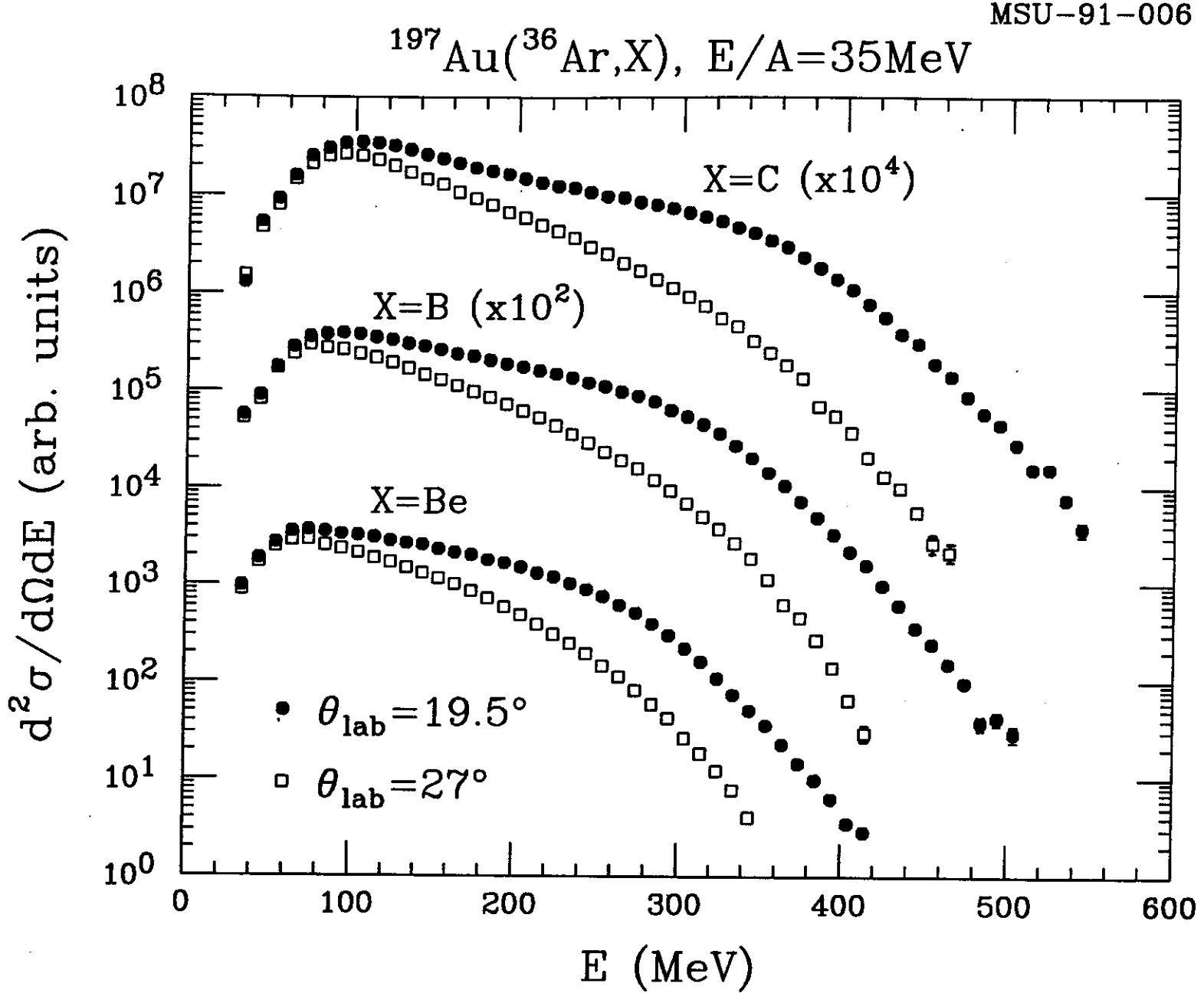
MSU-91-006
^{197}Au(^{36}Ar,X), E/A=35MeV
X=C (x10^4)
X=B (x10^2)
X=Be
θ_{lab}=19.5°
θ_{lab}=27°
d$^2\sigma$/dΩdE (arb. units)
E (MeV)
10^8
10^7
10^6
10^5
10^4
10^3
10^2
10^1
10^0
0
100
200
300
400
500
600

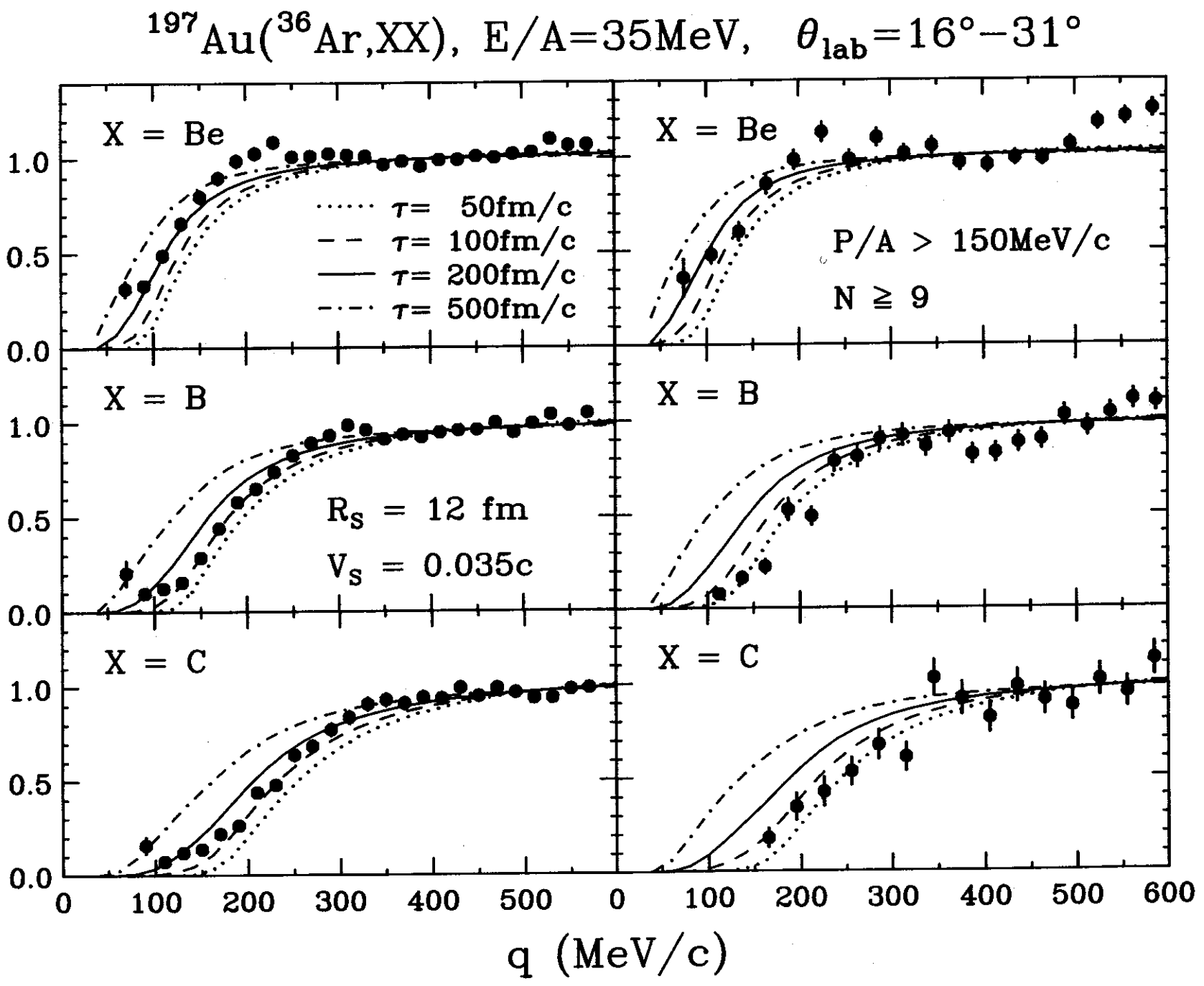
^{197}Au(^{36}Ar,XX), E/A=35MeV, θ_{lab}=16°–31°
X = Be
X = Be
τ= 50fm/c
τ= 100fm/c
τ= 200fm/c
τ= 500fm/c
P/A > 150MeV/c
N ≧ 9
X = B
X = B
R_s = 12 fm
V_s = 0.035c
X = C
X = C
1+R(q)
q (MeV/c)
0.0
0.5
1.0
0
100
200
300
400
500
600

Fig. 2

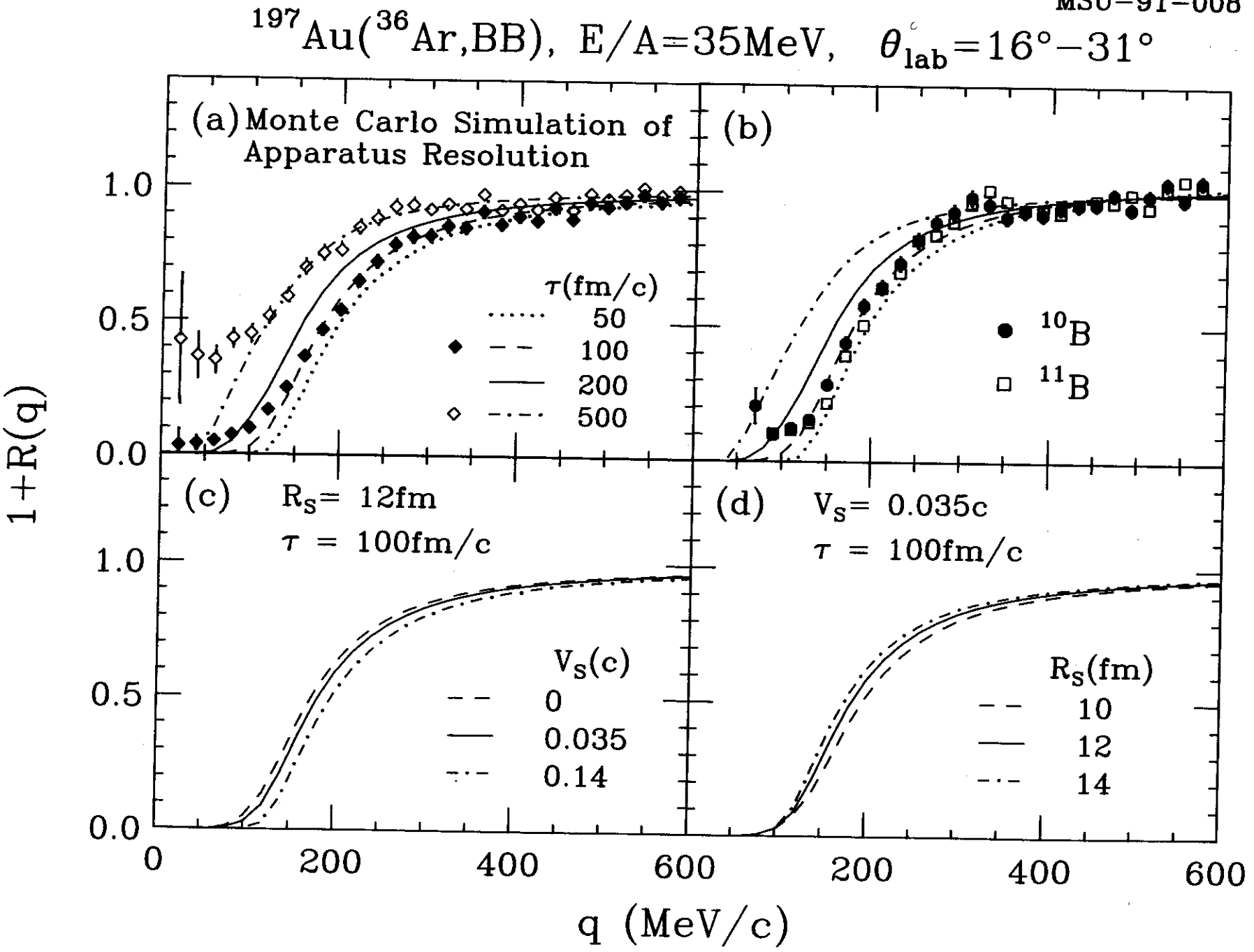
^{197}Au(^{36}Ar,BB), E/A=35MeV, θ_{lab}=16°−31°
(a) Monte Carlo Simulation of Apparatus Resolution
τ(fm/c)
50
100
200
500
(b)
^{10}B
^{11}B
(c) R_S= 12fm
τ = 100fm/c
V_S(c)
0
0.035
0.14
(d) V_S= 0.035c
τ = 100fm/c
R_S(fm)
10
12
14
1+R(q)
q (MeV/c)
0.0
0.5
1.0
0
200
400
600

Fig. 3

MSU-91-009

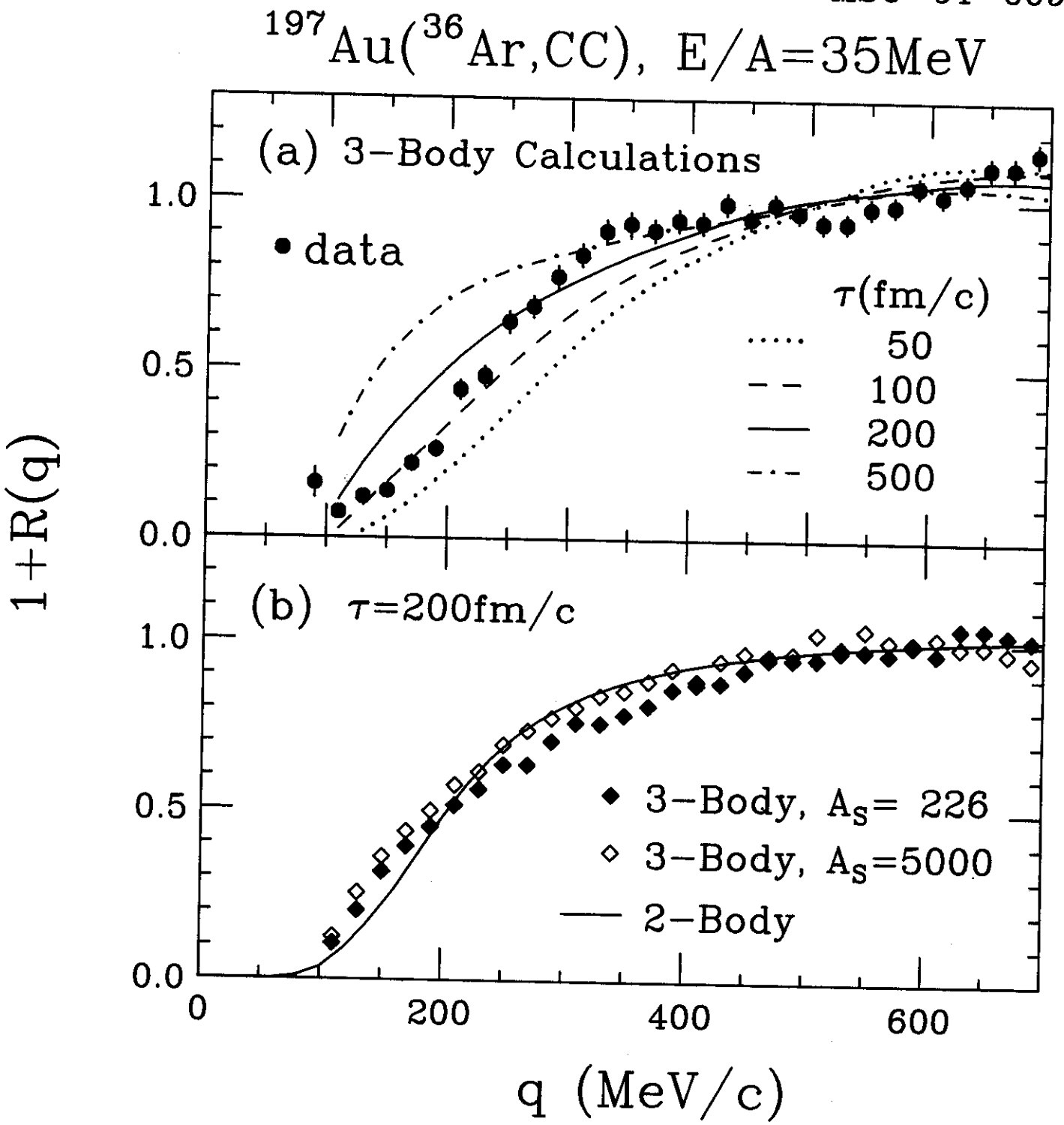

Fig. 4